VIBRATION SUPPRESSION CONTROL PROFILE GENERATION FOR HARD DISK DRIVE FLEXIBLE ARM LONG SEEK POSITION CONTROL

Li Zhou, Eduardo A. Misawa

School of Mechanical and Aerospace Engineering, Oklahoma State University, Stillwater, OK 74078-5016, USA

Abstract: A control profile is generated which suppresses all the resonant dynamics in a hard disk drive flexible arm. This control profile has both the drive voltage and velocity constraints which are required in hard disk drive long seek control. The control profile is generated from the sloped fast acceleration command and the vibration suppression shape filter technology. The simulation results for hard disk drive long seek control illustrate the effectiveness of the proposed method. *Copyright ©2005 IFAC*

Keywords: Flexible dynamic system, residual vibration control, hard disk drive actuator

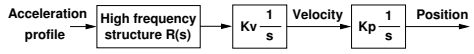

Fig. 1. A typical mechanical flexible system.

1. INTRODUCTION

Control of flexible structures has been extensively studied in recent years. Flexible structures such as high-speed disk drive actuators require extremely precise positioning under very tight time constraints. Whenever a fast motion is commanded, residual vibration in the flexible structure is induced, which increases the settling time. One solution is to design a closed-loop controller to damp out vibrations caused by the command inputs and disturbances to the plant. However, the resulting closed-loop response may still be too slow to provide an acceptable settling time, and the closed-loop control is not able to compensate for high frequency residual vibration which occurs beyond the closed-loop bandwidth. An alternative approach is to develop an appropriate reference trajectory that is able to minimize the excitation energy imparted to the system at its natural frequencies.

[1] Supported by the National Science Foundation, grant number 9978748, and Seagate Technology LLC of Oklahoma City, Oklahoma.

Fig. 1 shows a typical mechanical flexible system, where $\frac{1}{s}$ is an integrator, K_v is a velocity constant gain, and K_p is a position constant gain. The high frequency modes can be described as a transfer function $R(s) = \lim_{n\to\infty} \frac{b_n s^n + b_{n-1} s^{n-1} + \cdots + b_1 s + 1}{a_n s^n + a_{n-1} s^{n-1} + \cdots + a_1 s + 1}$ in which an infinite number of lightly damped resonant structures is possible. The goal of vibration suppression trajectory generation is to find a fast input trajectory, under some physical constraint, with minimum possible residual vibration.

In the previous study (Zhou and Misawa, 2005*b*), a control profile is generated which suppresses all the resonant dynamics in a flexible dynamic system. The proposed methods (Zhou and Misawa, 2005*b*) develop a vibration suppression control profile in the hard disk drive short seek control. In (Zhou and Misawa, 2005*c*), a vibration suppression control profile generation with both acceleration and velocity constraints is studied. The proposed method (Zhou and Misawa, 2005*c*) develops a vibration suppression control profile for hard disk drive long seek control. The control profile has both the drive current (or acceleration) and velocity constraints. In real application, the drive current does no saturate. It is the applied drive voltage that saturates. This paper presents a vibration suppression

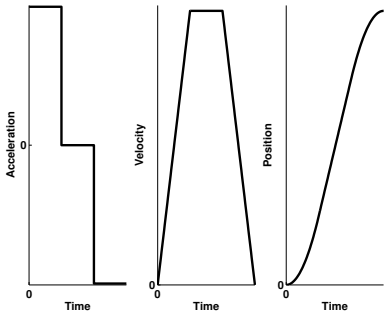

Fig. 2. Time-Optimal control profiles with both acceleration and velocity constraints.

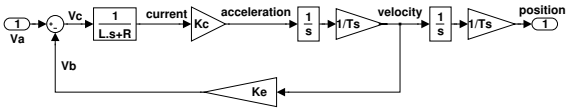

Fig. 3. The voice coil servo motor dynamics.

control profile generation method with both the drive applied voltage and velocity constraints.

2. LONG SEEK CONTROL PROFILE WITH BOTH APPLIED VOLTAGE AND VELOCITY CONSTRAINTS

For a purely rigid body, it can be inferred that the time-optimal acceleration profile with velocity constraint is composed by three parts. First, acceleration is commanded which always reaches the maximum limit. Secondly, when the maximum velocity is reached, the acceleration command becomes zero. In this situation, the rigid body is cruising with a constant velocity. The third part is a deceleration command which always reaches the minimum limit. Fig. 2 shows typical time-optimal control profiles with both acceleration and velocity constraints.

Fig. 3 shows a simplified hard disk drive voice coil servo motor dynamics. The applied voltage V_a is the sum of the control voltage V_c and the back-emf voltage V_b. The control voltage in terms of motor current command i is $V_c = Ri + L\frac{di}{dt}$, where L is the armature inductance and R is the armature resistance. The back-emf voltage in terms of the arm velocity vel is $V_b = K_e vel$, where K_e is the back-emf constant. Since the back-emf voltage is proportional to the velocity, a sloped acceleration command can be designed to overcome the effect of the back-emf voltage as shown in Fig. 4. The slope needs to be chosen such that the maximum allowable applied voltage is met for as long as possible but not saturated.

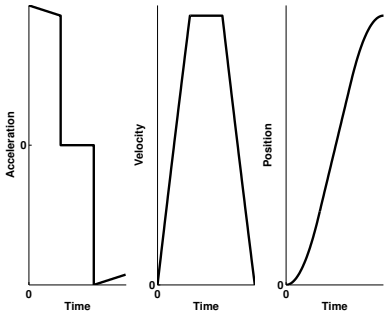

Fig. 4. Sloped fast control profiles with both acceleration and velocity constraints.

3. VIBRATION SUPPRESSION CONTROL PROFILE GENERATION WITH BOTH VOLTAGE AND VELOCITY CONSTRAINTS FOR A FLEXIBLE SYSTEM

In this section, a vibration suppression control profile generation with both applied voltage and velocity constraints for a flexible system is induced by using the vibration suppression shape filter technique (Zhou and Misawa, 2005*a*).

3.1 Calculating the Number of the Sloped Positive Acceleration Command Samples to Reach the Velocity Constraint

In this section, the number of the sloped positive acceleration command samples is calculated. The constraint of the acceleration $u[k]$ is assumed to be $|u[k]| \leq A_{max}$. The maximum velocity is assumed to be V_{max} and the sampling period is assumed to be T_s. The relationship between the acceleration command $u[k]$ and the velocity $v[k]$ is given as $\frac{V(z)}{U(z)} = K_a \frac{z^{-1}}{1-z^{-1}}$, where K_a is a constant gain. The difference equation between acceleration $u[k]$ at the discrete-time instant kT_s and velocity $v[k]$ at the discrete-time instant kT_s is given as $v[k] = K_a u[k-1] + v[k-1]$. If the initial velocity $v[0]$ is assumed to be zero, the velocity at the discrete-time instant kT_s can be computed as $v[k] = K_a \sum_{i=0}^{k-1} u[i]$.

The sloped positive acceleration command $u[k]$ is described as $u[k] = A_{max} - k \cdot S,\ k = 0, \cdots, m-1$, where S is the acceleration decrease per sample. As a result the following equation holds,

$$V_{max} = K_a \sum_{i=0}^{m-1} u[i] = K_a m \sum_{i=0}^{m-1} (A_{max} - i \cdot S),$$
$$= K_a (A_{max} + S/2)m - K_a S m^2/2.$$

Hence, m is the least positive solution of a second-order polynomial equation $K_a S m^2/2 - K_a(A_{max} + S/2)m + V_{max} = 0$. The number of the sloped positive acceleration command samples can be calculated as

$$m_1 = floor\,(m) \tag{1}$$

and the maximum velocity V_{rmax} from (1) is

$$V_{rmax} = K_a(A_{max}+S/2)m_1 - K_a S m_1^2/2 \le V_{max}. \quad (2)$$

3.2 Calculating the Number of the Zero Acceleration Command Samples

When the rigid body reaches the maximum velocity constraint described in (2), the rigid body is cruising at the constant velocity V_{rmax} as shown in Fig. 4. If the position movement is assumed to be P_{max}, the number of the zero acceleration command samples is calculated. The state-space model of the rigid body is described as $\begin{bmatrix} p[k+1] \\ v[k+1] \end{bmatrix} = G \begin{bmatrix} p[k] \\ v[k] \end{bmatrix} + K_b H u[k]$, where $G = \begin{bmatrix} 1 & T_s \\ 0 & 1 \end{bmatrix}$, $H = \begin{bmatrix} T_s^2/2 \\ T_s \end{bmatrix}$, $p[k]$ is the position at the discrete-time instant kT_s, $v[k]$ is the velocity at the discrete-time instant kT_s, and K_b is a constant gain. The acceleration command u has the following format

$$\begin{aligned} u = [&\underbrace{A_{max}, A_{max}-S, \cdots, A_{max}-(m_1-1)S}_{m_1}, \\ &\underbrace{0,\ 0, \cdots, 0}_{n}, \\ &\underbrace{-A_{max}, -(A_{max}-S)\cdots, -(A_{max}-(m_1-1)S)}_{m_1}]. \end{aligned}$$

If the initial position $p[0]$ and velocity $v[0]$ are assumed to be zero, the position and velocity at the discrete-time instant kT_s can be computed as (Ogata, 1995)

$$\begin{aligned} \begin{bmatrix} p[k] \\ v[k] \end{bmatrix} &= G^k \begin{bmatrix} p[0] \\ v[0] \end{bmatrix} + \sum_{i=0}^{k-1} G^i K_b H u[k-i-1], \\ &= \sum_{i=0}^{k-1} G^i K_b H u[k-i-1]. \end{aligned}$$

So at the discrete-time instant $(2m_1+n)T_s$,

$$\begin{aligned} \begin{bmatrix} p[2m_1+n] \\ v[2m_1+n] \end{bmatrix} &= \sum_{i=0}^{2m_1+n-1} G^i K_b H u[2m_1+n-i-1], \\ &= \begin{bmatrix} \frac{K_b m_1 T_s^2}{2}(2A_{max}+S-Sm_1)(m_1+n) \\ 0 \end{bmatrix}. \end{aligned}$$

If the position at the discrete-time instant $(2m_1+n)T_s$ is imposed to be P_{max}, i.e. $\frac{K_b m_1 T_s^2}{2}(2A_{max}+S-Sm_1)(m_1+n) = P_{max}$, then

$$n = \frac{2P_{max}}{K_b m_1 T_s^2 (2A_{max}+S-Sm_1)} - m_1. \quad (3)$$

Generally the above n is not an integer. Let $n = floor(n)+\alpha$, where $\alpha = n - floor(n)$ and $0 \le \alpha < 1$. The number of zero acceleration command samples can be chosen to be

$$n_1 = floor(n) + 1. \quad (4)$$

In the above implementation, since the resultant number of zero acceleration command n_1 is generally greater than the required fractional number of samples n, the resultant position at the end of the acceleration command is greater than the required position constraint which is P_{max}. Fig. 5 shows the calculated fractional number of the maximum velocity profile. The time interval between the final maximum velocity impulse V_{rmax} and the next velocity impulse b_0 is αT_s which is less than one sampling period T_s. Fig. 6 shows the modification of the integer number of the maximum velocity profile from (4). Compared with Fig. 5, the summation of velocity impulses in Fig. 6 is increased by $(1-\alpha)V_{rmax}$ per sample. The additional velocity impulse summation can be compensated for by slightly modifying the velocity impulses. The acceleration command corresponding the velocity profile in Fig. 6 is

$$\begin{aligned} u = [&\underbrace{A_{max}, A_{max}-S, \cdots, A_{max}-(m_1-1)S}_{m_1}, \\ &\underbrace{0,\ 0, \cdots, 0}_{n_1}, \\ &\underbrace{-A_{max}, -(A_{max}-S)\cdots, -(A_{max}-(m_1-1)S)}_{m_1}]. \end{aligned} \quad (5)$$

The velocity profile from (5) can be described as

$$\begin{aligned} v[0] &= 0, \\ v[k] &= K_a \sum_{i=0}^{k-1} u[i], k = 1, \cdots, 2m_1+n_1-1, \\ v[2m_1+n_1] &= 0. \end{aligned}$$

The above velocity profile can be modified to

$$\begin{aligned} v_1[0] &= 0, \\ v_1[k] &= v[k] - \frac{(1-\alpha)V_{rmax}}{2m_1+n_1-1}, \\ &\quad k = 1, \cdots, 2m_1+n_1-1, \\ v_1[2m_1+n_1] &= 0. \end{aligned}$$

The integral of the modified velocity impulses is exactly the same as the required integral of the velocity impulses in Fig. 5. The resultant modified acceleration command corresponding to (5) is

$$\begin{aligned} u_1[0] &= A_{max} - \frac{(1-\alpha)V_{rmax}}{K_a(2m_1+n_1-1)}, \\ u_1[k] &= u[k],\ k = 1, \cdots, 2m_1+n_1-1, \\ u_1[2m_1+n_1-1] &= -[A_{max} - \frac{(1-\alpha)V_{rmax}}{K_a(2m_1+n_1-1)}]. \end{aligned} \quad (6)$$

In (4), if the resultant integer number n_1 of the zero acceleration command is less than 0, then the acceleration and the velocity limits are not required to achieve the position constraint. In this situation, to guarantee the position constraint, either a reduced acceleration limit or a reduced velocity limit may be implemented. It is easy to understand that the resultant maximum

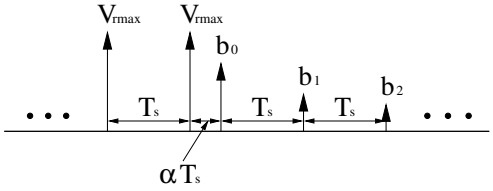

Fig. 5. The calculated fractional number of the maximum velocity profile.

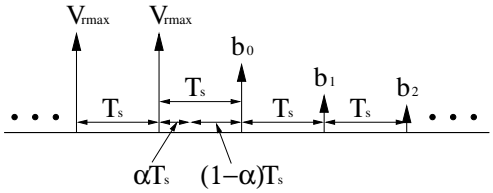

Fig. 6. The modification of the integer number of the maximum velocity profile.

Fig. 7. Generation of a vibration suppression command.

velocity from the modified acceleration command (6) is slightly less than V_{rmax} in (2).

3.3 Vibration Suppression Profile Generation with Both Acceleration and Velocity Constraints

Since the sloped fast acceleration command is generated in the previous section, a vibration suppression command can be generated as shown in Fig. 7. The vibration suppression command is the convolution of the sloped fast command and the vibration suppression shape filter. The vibration suppression shape filter in Fig. 7 is simply described in (Zhou and Misawa, 2005*a*). In (Zhou and Misawa, 2005*a*), it shows that the Input Shaping® [2] (Singer and Seering, 1990) is a special case of a non-continuous impulse function based vibration suppression shape filter. Different from the Input Shaping®, the vibration suppression shape filter in (Zhou and Misawa, 2005*a*) is generated from a continuous function, so it is able to suppress the high frequency resonance modes besides canceling the low frequence resonance modes. However, the Input Shaping® are not able to suppress the unmodeled high frequency vibrations if they are designed based on a low frequency resonance mode (Zhou and Misawa, 2005*a*).

4. SIMULATION RESULTS FOR HARD DISK DRIVE LONG SEEK CONTROL

Consider the following flexible system which is embedded in a hard disk assembly, $H(s) = K_c \cdot K_v \cdot K_p \cdot R(s)\frac{1}{s^2}$, where the input is the current signal in amps and the output is the position signal in tracks. The variable $K_c = 1.3\ \frac{\text{tracks/sample}^2}{\text{amp}}$ is a constant gain from current to acceleration, $K_v = 5 \times 10^4\ \frac{\text{samples}}{\text{sec}}$ is the velocity gain, $K_p = 5 \times 10^4\ \frac{\text{samples}}{\text{sec}}$ is the position gain, and $R(s)$ is a resonance structure. The Bode magnitude plot of a reduced order (28^{th}) $R(s)$ is shown in Fig. 8. This resonance transfer function $R(s)$ was derived from the flexible arm of an open disk drive at the Oklahoma State University Advanced Controls Laboratory. The resonance modes change drastically due to variation of the mode parameters. On the Bode plot, the peaks of the frequency response may shift both in frequency and in amplitude.

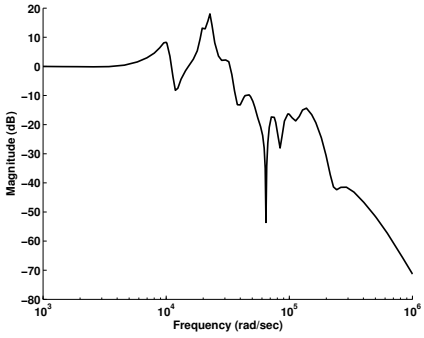

Fig. 8. Bode magnitude of the resonance structure.

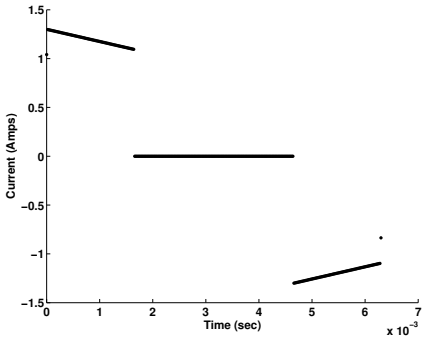

Fig. 9. Sloped fast current command with the velocity constraint.

The maximum velocity constraint is $V_{max} = 130$ tracks/sample, the applied voltage constraint is $V_a = 12$ volts, the long seek position movement is $P_{max} = 3 \times 10^4$ tracks, the sampling period is $T_s = 2 \times 10^{-5}$ seconds, the maximum current is chosen to be $A_{amx} = 1.3$ amp, and the slope value is chosen to be $S = 0.0025\ \frac{\text{tracks/sample}^2}{\text{sample}}$. Fig. 9 shows the sloped fast current command with the velocity constraint. Fig. 10 shows the resultant velocity signal. Fig. 11 shows the resultant position signal. Fig. 12 shows the position signal near the target track. The interval of Y axis in Fig. 12 is scaled to exactly 10 tracks and it shows that the residual vibration exists for a long period of time after the end of the current command (6.3 msec).

To suppress the residual vibration, a rectangle based shaper filter (Zhou and Misawa, 2005*a*) is designed based on the first resonance mode in the flexible

[2] Input Shaping® is a registered trademark of Convolve, Inc. in the United States.

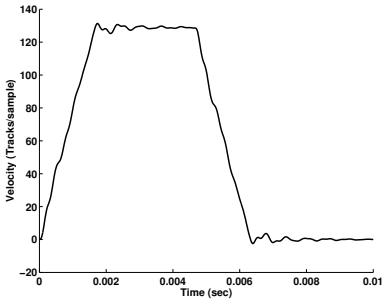

Fig. 10. The velocity signal with the sloped fast current.

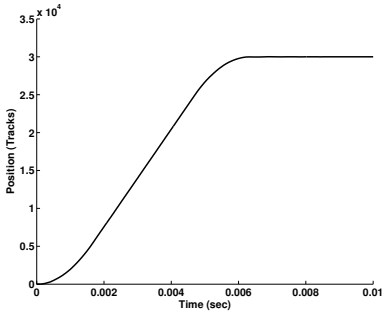

Fig. 11. The position signal with the sloped fast current command.

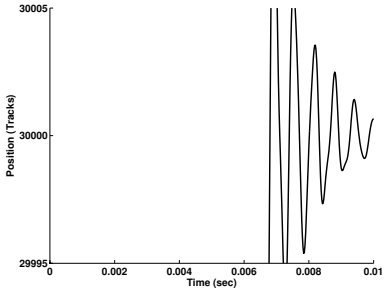

Fig. 12. The position signal near the target track.

system. The first resonance mode has the parameter $\omega_1 = 6.12 \times 10^3$ rad/sec and $\zeta_1 = 0.7$. Fig. 13 shows the resultant vibration suppression shape filter. Fig. 14 shows the vibration suppression current command. Fig. 15 shows the resultant velocity signal. Fig. 16 shows the resultant position signal near the target track. The interval of Y axis in Fig. 16 is scaled to exactly 10 tracks. Although the residual vibration due to the first resonance mode has been canceled, a large vibration still exists after the end of the current command. This residual vibration is caused by the second resonance mode in the flexible system.

To suppress the residual vibration of the second resonance mode, a rectangle based shaper filter (Zhou and Misawa, 2005*a*) is designed based on the second resonance mode in the flexible system. This mode has the parameter $\omega_1 = 1.02 \times 10^4$ rad/sec and $\zeta_1 = 0.08$. Fig. 17 shows the resultant vibration suppression shape filter based on the second resonance mode. Combining the shape filter in Fig. 13 and the shape filter in Fig. 17 results in a new shape filter as shown in Fig. 18. The resultant new vibration suppression shape

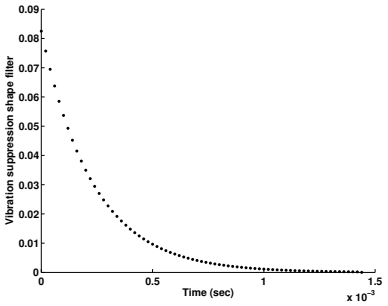

Fig. 13. Rectangle based shape filter based on resonance parameter $\omega_1 = 6.12 \times 10^3$ rad/sec and $\zeta_1 = 0.7$.

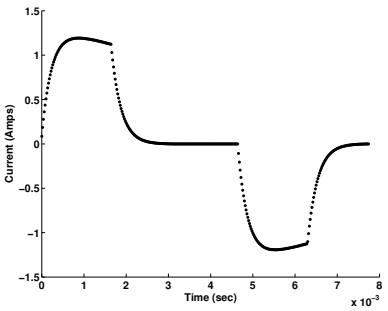

Fig. 14. Vibration suppression current command.

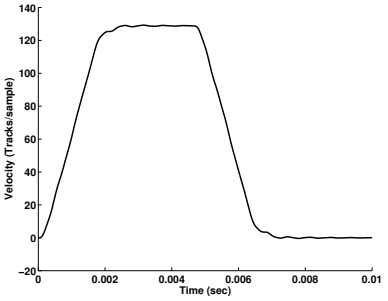

Fig. 15. Velocity signal with the vibration suppression current command.

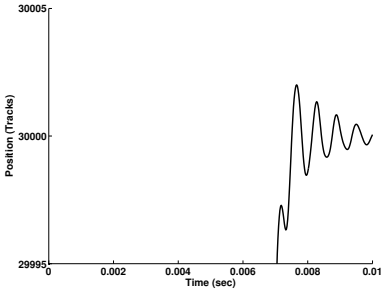

Fig. 16. Position signal near the target track.

filter in Fig. 18 cancels the residual vibration due to both the first and the second resonance modes. Fig. 19 shows the vibration suppression current command. Fig. 20 shows the resultant velocity signal. Fig. 21 shows the resultant position signal near the target track. The interval of Y axis in Fig. 21 is scaled to exactly 1 track. It is obvious that the residual vibration due to both the first and the second resonance modes is canceled and the residual vibration due to all the high

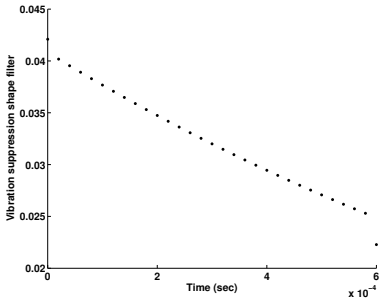

Fig. 17. Rectangle based shape filter based on resonance parameter $\omega_2 = 1.02 \times 10^4$ rad/sec and $\zeta_1 = 0.08$.

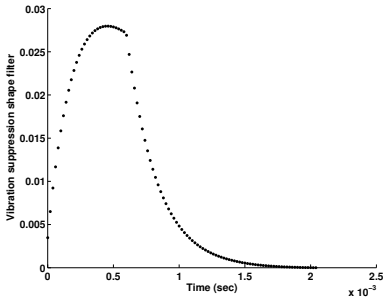

Fig. 18. Vibration suppression shape filter to cancel both the first resonance mode and the second resonance mode.

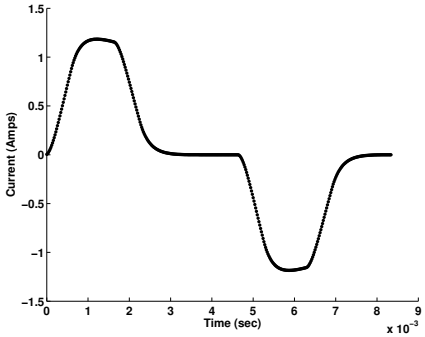

Fig. 19. Vibration suppression current command.

frequency modes is also suppressed. Fig. 22 shows the drive applied voltage signal due to the drive current command and it shows that the maximum allowable applied voltage is met but not saturated. The future work will include how to automatically select the slope parameter S and drive current limit A_{max} given the velocity, position and applied voltage constraints.

5. CONCLUSIONS

In this examination, a vibration suppression control profile is generated with both the drive voltage and velocity constraints. The simulation results of the hard disk drive long seek control show the effectiveness of this method. The proposed methods apply to other flexible dynamic system long seek control problem. The methods in this paper are patented (pending). Commercial use of these methods requires written permission from the Oklahoma State University.

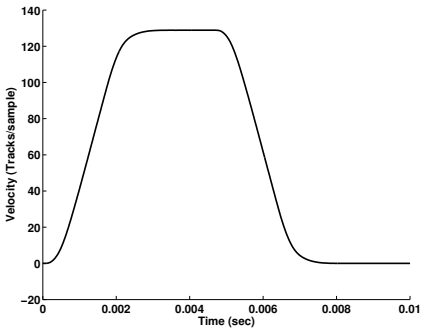

Fig. 20. Velocity signal with the vibration suppression current.

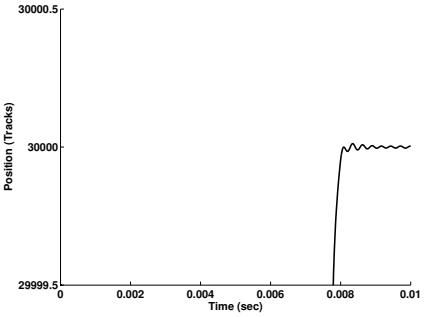

Fig. 21. Position signal near the target track.

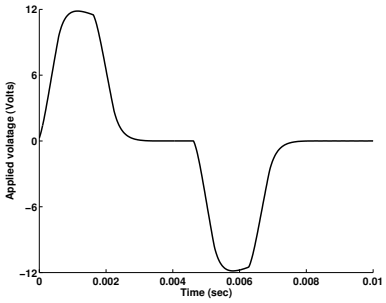

Fig. 22. Applied drive voltage signal due to the drive current command.

REFERENCES

Ogata, K. (1995). *Discrete-Time Control Systems*. Prentice Hall, Inc., Englewood Cliffs, NJ.

Singer, N. C. and W. P. Seering (1990). Preshaping command inputs to reduce system vibration. *ASME, Journal of Dynamic Systems, Measurement, and Control* **112**, 76–82.

Zhou, L. and E. A. Misawa (2005*a*). From Input Shaping ® and OATF to vibration suppression shape filter. *To appear in 2005 American Control Conference*.

Zhou, L. and E. A. Misawa (2005*b*). Generation of a vibration suppression control profile from optimal energy concentration functions. *To appear in 2005 American Control Conference*.

Zhou, L. and E. A. Misawa (2005*c*). Vibration suppression control profile generation with both acceleration and velocity constraints. *To appear in 2005 American Control Conference*.